

Cramer-Rao Type Bounds for Sparsity-Aware Multi-Sensor Multi-Target Tracking

Saurav Subedi, Yimin D. Zhang, Moeness G. Amin, and Braham Himed

Abstract

Conventionally, sparsity-aware multi-sensor multi-target tracking (MTT) algorithms comprise a two-step architecture that cascades group sparse reconstruction and MTT algorithms. The group sparse reconstruction algorithm exploits the *a priori* information that the measurements across multiple sensors share a common sparse support in a discretized target state space and provides a computationally efficient technique for centralized multi-sensor information fusion. In the succeeding step, the MTT filter performs the data association, compensates for the missed detections, removes the clutter components, and improves the accuracy of multi-target state estimates according to the pre-defined target dynamic model. In a recent work, a novel technique was proposed for sparsity-aware multi-sensor MTT that deploys a recursive feedback mechanism such that the group sparse reconstruction algorithm also benefits from the *a priori* knowledge about the target dynamics. As such, it is of significant interest to compare the tracking performance of these methods to the optimal multi-sensor MTT solution, with and without considering the missing samples. In this paper, we analytically evaluate the Cramer-Rao type performance bounds for these two schemes for sparsity-aware MTT algorithms and show that the recursive learning structure outperforms the conventional approach, when the measurement vectors are corrupted by missing samples and additive noise.

Index Terms

Performance bound, sparse reconstruction, multi-target tracking, recursive learning.

The work of S. Subedi, Y. D. Zhang, and M. G. Amin was supported in part by a subcontract with Defense Engineering Corporation for research sponsored by the Air Force Research Laboratory under Contract FA8650-12-D-1376. The work of Y. D. Zhang is also supported in part by a subcontract with Matrix Research, Inc. for research sponsored by the Air Force Research Laboratory under contract FA8650-14-D-1722. Part of the results was presented at the 2016 IEEE Radar Conference [1].

S. Subedi and M. G. Amin are with the Center for Advanced Communications, Villanova University, Villanova, PA 19085, USA.

Y. D. Zhang is with the Department of Electrical and Computer Engineering, Temple University, Philadelphia, PA 19122, USA (e-mail: ydzhang@temple.edu).

B. Himed is with the RF Technology Branch, Air Force Research Laboratory, AFRL/RVMD, Dayton, OH 45433, USA.

I. INTRODUCTION

In recent years, sparsity-aware multi-target tracking (MTT) algorithms have attracted significant research interest. Researchers have proposed several techniques (e.g., [2–5]) to exploit the *a priori* knowledge that there is only a small number of targets to be tracked over a pre-defined surveillance area, and hence, the measurements are sparse, either in their natural basis or some other sparsifying basis. Recently, the hierarchical Kalman filter has been proposed in [6] to track the dynamic sparse signals, which incorporates the fundamentals of sparse Bayesian learning into the traditional Kalman filtering, where the output of the tracking filter is exploited to update the covariance matrix of the process noise, thereby enforcing sparsity constraint into the traditional Kalman filtering framework.

Conventionally, the sparsity-aware MTT algorithm cascades the sparse signal reconstruction algorithm and the multi-target tracking algorithm in succession. First, the sparse reconstruction algorithm is exploited to estimate the multi-target state, and in the succeeding step, multi-target state estimates are fed as inputs to the MTT filters for data association, clutter removal, compensation for missed detections, and reduction in the localization error. For multi-sensor MTT [7], group sparse reconstruction algorithms have been deployed as computationally efficient techniques for a centralized multi-sensor information fusion. The *a priori* information that the measurements across multiple sensors share a common sparse support in a discretized target state space allows for the exploitation of the group sparse reconstruction. As such, the output of the group sparse reconstruction algorithm obtained in the form of instantaneous estimates of the multi-target states is fed as the input to the MTT filters. The overall performance of these techniques relies on the ability of the group sparse reconstruction algorithm to accurately and reliably estimate the instantaneous multi-target states.

In many practical applications, the observations suffer from a high proportion of missing samples, due to fading, shadowing or removal of impulsive noise, and is corrupted by a strong additive noise, rendering it difficult to accurately estimate the multi-target states using group sparse reconstruction-based methods. Recently, a novel technique is proposed in [8] for sparsity-aware multi-sensor MTT that deploys a recursive feedback mechanism such that the group sparse reconstruction algorithm and the conventional MTT filter interplay and learn from each other. Such recursive learning approach creates a global learning architecture that enables the group sparse reconstruction algorithm to benefit from the *a priori* knowledge about the target dynamics. Numerical results presented in [8] in terms of the optimal sub-pattern assignment (OSPA) metric [9] show that the methods proposed therein enable a significant performance improvement over the conventional approach through such a feedback mechanism. This is particularly evident when the measurement vectors comprise a high percentage of missing samples and

are corrupted by strong additive noise.

The unconditional posterior Cramer-Rao lower bound (PCRLB) [10] provides a theoretical performance limit of any estimator for a non-linear filtering problem under the Bayesian framework. In [11], the authors derived a recursive approach to calculate the sequential PCRLB for a general multi-dimensional discrete-time non-linear filtering problem. Several variants of the PCRLB have been proposed in the literature to make the PCRLB more adaptive. For instance, in [12–14], the PCRLB is conditioned on the measurements up to a reset initial time in lieu of the absolute initial state as in the vanilla PCRLB definition. Instead of representing the posterior probability density function of the system state at the reset initial time non-parametrically by a set of random particles as in [12], a systematic recursive approach is used to derive the exact conditional PCRLB based on first principles in [15]. Two other online conditional PCRLBs are proposed in [16] as alternatives to the one proposed in [15], and are shown to provide similar results through numerical examples. These variants have rendered the prior knowledge of the initial system state more useful and relevant in the PCRLB evaluation, particularly in situations when the state process noise is high and thus the prior knowledge regarding the system state at the initial time quickly becomes irrelevant. However, to the best of our knowledge, none of the existing works provide a conditional PCRLB for situations where the measurement is unreliable due to strong additive noise and/or a high proportion of missing samples. As such, the existing literature still lacks the PCRLB analysis for sparsity-aware multi-sensor MTT problems.

In this paper, we analytically evaluate the performance bounds, for the two aforementioned architectures for sparsity-aware multi-sensor MTT, namely, the conventional architecture and the global learning architecture. We quantify the degradation in the overall tracking performance when the measurement vectors suffer from a high percentage of missing samples and strong additive noise. First, we derive the performance bounds for the estimation of the instantaneous multi-target state exploiting the group sparse signal reconstruction algorithm in the case of a signal model comprising missing samples and additive white Gaussian noise perturbation [17]. Assuming an optimal estimation of the instantaneous multi-target state by the group sparse reconstruction algorithm under the given signal conditions, we evaluate the performance bound for the MTT algorithm. Next, we analytically evaluate the performance improvement achieved by implementing the recursive learning architecture, where the *a priori* knowledge about the target dynamics is exploited at the sparse reconstruction stage through a feedback mechanism. To summarize, the key contributions of this paper are follows:

- 1) We analytically quantify the effect of missing samples and additive noise on the performance of sparsity-aware multi-sensor MTT algorithms.

- 2) We evaluate the limits on the performance improvement that can be achieved by implementing the recursive learning architecture assuming optimal estimation at both stages - group sparse reconstruction and MTT.
- 3) We analyze the boundary conditions for which the recursive learning architecture guarantees a convergence and assess the effect of relative weight on the achievable performance improvement.

The remainder of the paper is organized as follows. Section II describes the target dynamic model, presents the signal model, considering the effect of missing samples and additive white Gaussian noise. Section III presents a high-level overview of the two approaches for sparsity-aware MTT. Section IV presents the analytical comparison of the performance bounds for these two approaches. Section V provides simulation results in the case of a multi-target tracking in a multi-static passive Doppler sensor network, and finally conclusions are drawn in Section VI.

Notations: A lower (upper) case bold letter denotes a vector (matrix). Specifically, \mathbf{I}_N and $\mathbf{0}_N$ denote the $N \times N$ identity and zero matrices, respectively. $(\cdot)^T$ and $(\cdot)^H$, respectively, denote transpose and Hermitian operations, and \circ denotes the Hadamard product. $\text{diag}(\cdot)$ forms a diagonal matrix from a vector, $\text{tr}(\cdot)$ stands for matrix trace, and $\text{Re}(\cdot)$ denotes the real part of a complex variable. $\mathbb{E}(\cdot)$ stands for the expectation operation. $\mathbb{C}^{m \times n}$ and $\mathbb{C}^{m \times 1}$ represent an $m \times n$ -dimensional complex matrix and an m -element complex vector, respectively. Likewise, $\mathbb{R}^{m \times 1}$ represents an m -element real vector. $\|\cdot\|_n$ denotes the l_n -norm of a vector, and $x \sim \mathcal{N}(a, b)$ and $x \sim \mathcal{CN}(a, b)$, respectively, denote variable x to be real and complex Gaussian distributed with mean a and variance b .

II. SIGNAL MODEL

A. Target dynamics

We consider the problem of tracking K moving targets, where K is unknown. The ground truth state vector associated with the k th target at the t th observation instant is represented as $\boldsymbol{\theta}_{t,k} \in \mathbb{R}^{D \times 1}$, for $k = 1, \dots, K$ and $t = 1, \dots, T$. Herein, we refer to the observation instants as the time instants at which the sensors report their measurement vectors to the fusion center. Note that each measurement comprises several discrete-time samples of the waveform received at the sensor. The number of samples per measurement vector depends on the observation interval and the sampling rate deployed at the sensor. At each observation instant, the ground truth state set is defined as $\boldsymbol{\Theta}_t \triangleq [\boldsymbol{\theta}_{1,t}^T, \dots, \boldsymbol{\theta}_{K,t}^T]^T$. The target dynamics is assumed to evolve according to a linear Gaussian model, such that

$$\boldsymbol{\theta}_{t,k} = \mathbf{F}\boldsymbol{\theta}_{t-1,k} + \mathbf{w}_{t,k}, \quad (1)$$

where \mathbf{F} is the state transition matrix and $\mathbf{w}_{t,k} \sim \mathcal{N}(\mathbf{0}, \mathbf{Q})$ is the process noise modeled as additive white Gaussian. The definitions of the state transition matrix \mathbf{F} and the covariance matrix of the process noise \mathbf{Q} depend on the application. Application examples will be provided in Section V.

B. Observation with missing samples

We consider R receivers monitoring the region of interest. The multi-target states are represented as a multi-component signal in the observation space at the r th receiver through a deterministic mapping, such that

$$\check{x}_t^{(r)}(m) = \sum_{k=1}^K s_{t,k}^{(r)} \psi^{(r)}(\boldsymbol{\theta}_{t,k}, m), \quad (2)$$

where $\check{x}_t^{(r)}(m)$ is the m th sample in the observation domain, $m = 0, \dots, M-1$, $s_{t,k}^{(r)}$ is the amplitude of the signal corresponding to the k th target and $\psi^{(r)}(\cdot)$ is the deterministic, possibly a non-linear, mapping function.

In most tracking applications, the entire target state space, comprising N possible target states, can be discretized and represented as an N -dimensional vector $\mathbf{s}_t^{(r)}$ corresponding to each receiver indexed as $r = 1, \dots, R$, such that each element in $\mathbf{s}_t^{(r)}$ is uniquely associated with a possible target state either directly in its natural state or through a deterministic mapping. Since the total number of targets within the surveillance region at the t th observation is K , where $K \ll N$, the entire target state space can be represented by a K -sparse vector $\mathbf{s}_t^{(r)} \in \mathbb{C}^{N \times 1}$, i.e., $\|\mathbf{s}_t^{(r)}\|_0 = K$.

Following a typical sparse signal reconstruction model, a sparse decomposition of an M -dimensional complex vector $\check{\mathbf{x}}_t^{(r)} \triangleq [\check{x}_t^{(r)}(0), \dots, \check{x}_t^{(r)}(M-1)]^T \in \mathbb{C}^{M \times 1}$ can be expressed as the linear model

$$\check{\mathbf{x}}_t^{(r)} = \boldsymbol{\Psi}_t^{(r)} \mathbf{s}_t^{(r)}, \quad (3)$$

where $\boldsymbol{\Psi}_t^{(r)} \in \mathbb{C}^{M \times N}$, $M \ll N$, represents the basis or the dictionary which relates the vector $\check{\mathbf{x}}_t^{(r)}$ to the sparse vector $\mathbf{s}_t^{(r)}$ according to a pre-defined model.

In many applications, the observation may suffer from a high proportion of missing samples due to propagation impairments resulting in fading or shadowing. Consider L samples missing from the $\mathbb{C}^{M \times 1}$ vector $\check{\mathbf{x}}_t^{(r)}$, where $0 \leq L < M$. The missing sample positions are assumed to be random and uniformly distributed over time. Accounting for the missing samples, we define the following observation vector $\mathbf{x}_t^{(r)}$,

$$\mathbf{x}_t^{(r)} = \check{\mathbf{x}}_t^{(r)} \circ \boldsymbol{\phi}_t^{(r)}, \quad (4)$$

where $\phi_t^{(r)} = [\phi_t^{(r)}(0), \dots, \phi_t^{(r)}(M-1)]^T$ with each element defined as an independent Bernoulli random variable with a success probability $(M-L)/M$ and a failure probability L/M . It is noted that the missing sample positions may be different at each observation interval and across each sensor. As such,

$$\phi_t^{(r)}(m) = \begin{cases} 1, & \text{if } m \in \mathcal{S}_t^{(r)}, \\ 0, & \text{otherwise,} \end{cases} \quad (5)$$

with $\mathcal{S}_t^{(r)} \subset \{0, \dots, M-1\}$ denoting the set of observed time instants and its cardinality is $|\mathcal{S}_t^{(r)}| = M-L$. Incorporating the missing samples, from (3) and (4), the actual observation can be expressed as

$$\mathbf{y}_t^{(r)} = \mathbf{\Phi}_t^{(r)} \check{\mathbf{x}}_t^{(r)} + \boldsymbol{\epsilon}_t^{(r)} = \mathbf{\Phi}_t^{(r)} \mathbf{\Psi}_t^{(r)} \mathbf{s}_t^{(r)} + \boldsymbol{\epsilon}_t^{(r)}, \quad (6)$$

where $\mathbf{\Phi}_t^{(r)} \triangleq \text{diag}(\phi_t^{(r)})$ and $\boldsymbol{\epsilon}_t^{(r)} \sim \mathcal{CN}(\mathbf{0}, \sigma_\epsilon^2 \mathbf{I}_M)$ is the thermal noise modeled as an additive Gaussian random vector.

C. Statistical model

Following the signal model in (6), the probability density function (pdf) of $\mathbf{y}_t^{(r)}$, conditioned on $\mathbf{\Phi}_t^{(r)}$ and the unknown ground truth state set Θ_t , is given as

$$p(\mathbf{y}_t^{(r)} | \mathbf{\Phi}_t^{(r)}, \Theta_t) \sim \mathcal{CN}(\mathbf{\Phi}_t^{(r)} \mathbf{\Psi}_t^{(r)} \mathbf{s}_t^{(r)}, \sigma_\epsilon^2 \mathbf{I}_M). \quad (7)$$

As such, the joint conditional pdf of the measurements from R independent receivers is expressed as

$$p(\mathbf{Y}_t | \mathbf{\Phi}_t, \Theta_t) \sim \prod_{r=1}^R \mathcal{CN}(\mathbf{\Phi}_t^{(r)} \mathbf{\Psi}_t^{(r)} \mathbf{s}_t^{(r)}, \sigma_\epsilon^2 \mathbf{I}_M), \quad (8)$$

where $\mathbf{Y}_t = [\mathbf{y}_t^{(1)}, \dots, \mathbf{y}_t^{(R)}]$ and $\mathbf{\Phi}_t = [\mathbf{\Phi}_t^{(1)}, \dots, \mathbf{\Phi}_t^{(R)}]$.

The mathematical structure of the optimal solution for multi-sensor MTT has been well analyzed [18, 19]. However, due the combinatorial complexity associated with the optimal solution [20, 21], a direct implementation of the optimal solution is impractical and several sub-optimal solutions have been proposed [22–24, 36]. Sparsity-aware multi-sensor MTT algorithms exploit group sparse reconstruction methods for a centralized multi-sensor information fusion [7, 8], and thus, significantly reduce the overall computational cost. In the following, we provide a high-level description of two commonly used approaches for sparsity-aware multi-sensor MTT, respectively introduced in [7] and [8].

III. SPARSITY-AWARE MULTI-TARGET TRACKING

Estimation of instantaneous multi-target states exploiting group sparse reconstruction is a fundamental step in sparsity-aware multi-sensor MTT. This provides a computationally tractable method to

simultaneously utilize the measurements available at all sensors by exploiting the group sparsity of the measurements in a discretized target state space.

A typical sparse signal reconstruction model is given as

$$\mathbf{g} = \mathbf{A}\boldsymbol{\theta} + \boldsymbol{\eta}, \quad (9)$$

where $\mathbf{g} \in \mathbb{R}^{P \times 1}$ is a measurement vector, $\mathbf{A} \in \mathbb{R}^{P \times Q}$, $P \ll Q$, is a known dictionary matrix, $\boldsymbol{\theta} \in \mathbb{R}^{Q \times 1}$ is the unknown sparse weight vector to be estimated, and $\boldsymbol{\eta} \in \mathbb{R}^{P \times 1}$ is the additive white Gaussian noise vector modeled as $\boldsymbol{\eta} \sim \mathcal{N}(\mathbf{0}, \sigma^2 \mathbf{I})$. The fundamental idea behind the sparsity based signal reconstruction is the fact that the measurement vector \mathbf{g} can be represented as a linear combination of K basis vectors in its natural basis or some other sparsifying basis, where $K \ll P$ [25].

In many practical applications, there are multiple measurements arising from a common physical phenomenon. In such cases, for a correctly chosen sparsifying basis, the sparse weight vectors share a common sparse support. Mathematically, such problems are modeled as

$$\mathbf{g}^{(n)} = \mathbf{A}^{(n)}\boldsymbol{\theta}^{(n)} + \boldsymbol{\eta}^{(n)}, \quad n \in [1, \dots, N], \quad (10)$$

where the sparse weight vectors $\boldsymbol{\theta}^{(n)}$ share the same sparsity support, whereas their values are generally different [26, 27]. Group sparse reconstruction has found applications in a wide range of multi-sensor problems, including direction-of-arrival estimation [28, 29], sensor selection [30], and multi-sensor MTT [7, 8]. There are a number of algorithms available to solve the group sparse problems such as group basis pursuit [31], group LASSO [32], and block orthogonal matching pursuit [33]. The multi-task Bayesian compressive sensing algorithm [34, 35] provides an adaptive learning framework and generally outperforms the conventional compressive sensing algorithms.

In the underlying problem, it is known *a priori* that the targets are sparsely distributed in the discretized target state space for any given observation instant t . This motivates us to reformulate the problem as a sparse reconstruction problem. Some recent works have proposed the exploitation of the prior knowledge about the sparsity of the signal to improve the tracking performance (e.g., sparsity-aware Kalman tracking [5] and hierarchical Bayesian Kalman filters [6]). In addition, we know *a priori* that the measurements received at R different receivers are generated due to the same set of targets within the surveillance region. As such, the measurements share a common sparse support in the discretized target state space, thus inviting the use of group sparse reconstruction for estimating the instantaneous multi-target state.

The conventional approach for sparsity-aware MTT [7] cascades the sparse reconstruction algorithm and the MTT filter as shown in Fig. 1. For every observation interval t , the solution of the group sparse reconstruction algorithm converges to a \hat{K} -sparse solution, whose indices correspond to the estimates

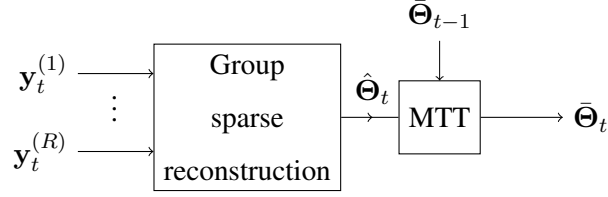


Fig. 1. Diagram of the conventional approach.

of the \hat{K} state vectors, $\hat{\theta}_{t,k}$, where $k = 1, \dots, \hat{K}$. As such, at every t , we obtain instantaneous multi-target state estimates, i.e., $\hat{\Theta}_t = [\hat{\theta}_{t,1}^T, \dots, \hat{\theta}_{t,\hat{K}}^T]^T$. Note that \hat{K} generally differs from K because of missed detections and false alarms. In the succeeding step, these instantaneous multi-target state estimates $\hat{\Theta}_t = [\hat{\theta}_{t,1}^T, \dots, \hat{\theta}_{t,\hat{K}}^T]^T$ are fed as inputs to the MTT filter. The output of the MTT filter, at every k , is denoted as $\bar{\Theta}_t = [\bar{\theta}_{t,1}^T, \dots, \bar{\theta}_{t,\bar{K}}^T]^T$, where \bar{K} is the estimated number of targets at the output of the MTT filter. In general, the MTT filter successfully compensates for the missed detections and removes the false alarms, thereby achieving a better estimate of the number of targets. As a result and upon convergence, \bar{K} is usually equal, or at least very close, to K .

The performance of the conventional approach is severely degraded when the measurements include a high proportion of missing samples and are corrupted by strong additive noise. A global learning structure has recently been proposed in [8] to provide an effective solution in such challenging conditions. The key idea behind the global learning architecture is that information from the MTT filter is exploited as an additional prior in each recursion at the sparse reconstruction stage. The conversion of multi-target state estimates obtained at the output of the MTT filter to the predicted measurement vectors in time-domain involves two deterministic steps, referred to as ‘reconstruction’ and ‘mapping’ in Fig. 2. Reconstruction involves populating a vector representing the discretized state space at the indices corresponding to the multi-target state estimates. Since the number of target state estimates $\bar{K} \ll N$, the resulting vector is a sparse vector. The mapping process involves the conversion of the sparse vector to predicted measurement vectors through a pre-defined deterministic model. As such, by recursively feeding the information from the MTT as an additional input to the group sparse reconstruction algorithm, both the sparse reconstruction algorithm and MTT filter recursively learn from each other, as shown in Fig. 2. The recursive process continues to refine the overall performance by reducing both the cardinality error and localization error until a convergence criterion is satisfied.

In the following, we analytically compare the performance bounds that can be achieved using these two approaches.

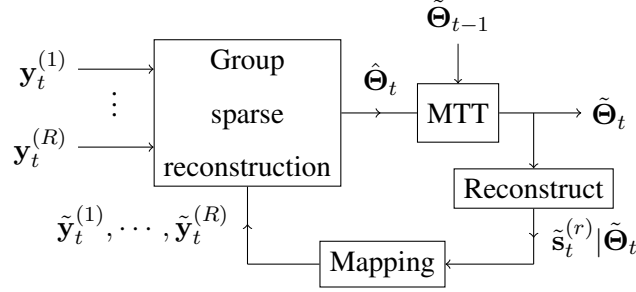


Fig. 2. Diagram of the recursive learning algorithm.

IV. PERFORMANCE BOUNDS

A. Conventional method

Following the statistical model in (8), where the observation vector comprising the missing samples is defined as a complex Gaussian variable with mean vector corresponding to the r th receiver $\boldsymbol{\mu}_t^{(r)} = \mathbb{E}\{\boldsymbol{\Phi}_t^{(r)} \boldsymbol{\Psi}_t^{(r)} \mathbf{s}_t^{(r)}\}$ and covariance matrix $\mathbf{C} = \sigma_\epsilon^2 \mathbf{I}_M$, the Fisher information matrix (FIM) $\mathcal{I}(\boldsymbol{\theta}_t)$ is given as [37]

$$\mathcal{I}(\boldsymbol{\theta}_t) = \mathbb{E} \left\{ \frac{\partial \ln p(\mathbf{Y}_t | \boldsymbol{\Phi}_t, \boldsymbol{\theta}_t)}{\partial \boldsymbol{\theta}_t} \frac{\partial \ln p(\mathbf{Y}_t | \boldsymbol{\Phi}_t, \boldsymbol{\theta}_t)^T}{\partial \boldsymbol{\theta}_t} \right\}. \quad (11)$$

Fundamentally, the target state estimation problem is analogous to the parameter estimation problem in multi-component polynomial phase signals [38]. The interactions among the multiple components or the cross-terms have a significant effect on the Cramer-Rao bound in such problems. Mathematically, such an effect is manifested through the off-diagonal blocks of the FIM. The closer the components in the estimation space, the larger the off-diagonal blocks are. As such, the estimation performance for each component is worse than the one achieved in a single-component case [39]. Herein, for analytical convenience, we resort to a commonly adopted assumption in MTT problems (e.g., [11, 23, 24, 43]) that each target evolves independent of each other and, therefore, is well-separated in the target state space from any other neighboring target. Since the target state vectors are assumed independent, the FIM is block diagonal in structure, and the (i, j) th block of the FIM is given by

$$[\mathcal{I}(\boldsymbol{\theta}_t)]_{ij} = R \operatorname{tr} \left\{ \frac{\partial \mathbf{C}^H}{\partial \boldsymbol{\theta}_{t,i}} \mathbf{C}^{-1} \frac{\partial \mathbf{C}}{\partial \boldsymbol{\theta}_{t,j}} \mathbf{C}^{-1} \right\} + \sum_{r=1}^R 2 \operatorname{Re} \left[\frac{\partial (\boldsymbol{\mu}_t^{(r)})^H}{\partial \boldsymbol{\theta}_{t,i}} \mathbf{C}^{-1} \frac{\partial \boldsymbol{\mu}_t^{(r)}}{\partial \boldsymbol{\theta}_{t,j}} \right]. \quad (12)$$

Since the unknown variables under consideration are the target state vectors, the first term in (12) vanishes to zero because the covariance matrix is independent of the target state vectors. As such, substituting for

the values of the mean vector $\boldsymbol{\mu}_t^{(r)}$ and the covariance matrix \mathbf{C} , we obtain

$$[\mathcal{I}(\boldsymbol{\theta}_t)]_{ij} = \sum_{r=1}^R 2\sigma_\epsilon^{-2} \text{Re} \left[\frac{\partial \text{E}\{(\mathbf{s}_t^{(r)})^H (\boldsymbol{\Psi}_t^{(r)})^H\}}{\partial \boldsymbol{\theta}_{t,i}} \boldsymbol{\Lambda} \frac{\partial \text{E}\{\boldsymbol{\Psi}_t^{(r)} \mathbf{s}_t^{(r)}\}}{\partial \boldsymbol{\theta}_{t,j}} \right], \quad (13)$$

where $\boldsymbol{\Lambda} = \text{E}\{\boldsymbol{\Phi}_t^H \boldsymbol{\Phi}_t\} = \text{E}\{\boldsymbol{\Phi}_t\} = [(M-L)/M] \mathbf{I}_M$. Thus, (13) becomes

$$[\mathcal{I}(\boldsymbol{\theta}_t)]_{ij} = \frac{2(M-L)}{M} \sigma_\epsilon^{-2} \sum_{r=1}^R \text{Re} \left[\frac{\partial \text{E}\{(\mathbf{s}_t^{(r)})^H (\boldsymbol{\Psi}_t^{(r)})^H\}}{\partial \boldsymbol{\theta}_{t,i}} \cdot \frac{\partial \text{E}\{\boldsymbol{\Psi}_t^{(r)} \mathbf{s}_t^{(r)}\}}{\partial \boldsymbol{\theta}_{t,j}} \right]. \quad (14)$$

On the other hand, when there are no missing samples, $\boldsymbol{\Lambda} = \mathbf{I}_M$. In this case, the (i, j) th block of the FIM is expressed as

$$[\mathcal{I}(\boldsymbol{\theta}_t)]_{ij} = 2\sigma_\epsilon^{-2} \sum_{r=1}^R \text{Re} \left[\frac{\partial \text{E}\{(\mathbf{s}_t^{(r)})^H (\boldsymbol{\Psi}_t^{(r)})^H\}}{\partial \boldsymbol{\theta}_{t,i}} \cdot \frac{\partial \text{E}\{\boldsymbol{\Psi}_t^{(r)} \mathbf{s}_t^{(r)}\}}{\partial \boldsymbol{\theta}_{t,j}} \right]. \quad (15)$$

Assuming that the ground truth state of each target is independent, the FIM assumes a block diagonal structure and, therefore, the CRLB on the variance of the unbiased estimator of $\boldsymbol{\theta}_{t,i}$ can be extracted as the inverse of the corresponding block of the FIM. Thus, by comparing (14) and (15), it becomes apparent that the loss of information due to the missing samples results in an increase in the variance of the estimated target state vectors by a factor of $M/(M-L)$.

In the conventional approach for sparsity-aware MTT, we use the estimates of the group sparse signal reconstruction algorithm $\hat{\boldsymbol{\Theta}}_t \triangleq [\hat{\boldsymbol{\theta}}_{t,1}^T, \dots, \hat{\boldsymbol{\theta}}_{t,K}^T]^T$ as inputs to the MTT filter. Since the purpose of this paper is to evaluate and compare the performance bounds, we consider that an optimal solution is attained from the group sparse reconstruction stage. There are several The covariance matrix of the inputs to the MTT filter can, therefore, be modeled as

$$\hat{\boldsymbol{\theta}}_{t,k} \sim \mathcal{N}(\boldsymbol{\theta}_{t,k}, [\mathcal{I}(\boldsymbol{\theta}_t)]_{kk}^{-1}). \quad (16)$$

The posterior FIM is calculated as a sum of a data matrix and a priori matrix [10, 40, 41]. Following the target dynamic model in (1) and the measurement model in (16), the recursive FIM can be expressed as

$$[\mathcal{I}(\bar{\boldsymbol{\theta}}_{t+1})]_{kk} = [\mathcal{I}(\boldsymbol{\theta}_{t+1})]_{kk} + [\mathbf{Q} + \mathbf{F}[\mathcal{I}(\bar{\boldsymbol{\theta}}_t)]_{kk} \mathbf{F}^T]^{-1}. \quad (17)$$

As such, the posterior bound on the variance of the estimator of the unknown ground truth state vectors at the t th observation is given as the inverse of the posterior FIM.

B. Recursive learning architecture

In the recursive learning architecture as shown in Fig. 2, there is information available in the form of predicted observation vectors $\{\tilde{\mathbf{y}}_t^{(1)}, \dots, \tilde{\mathbf{y}}_t^{(R)}\}$ from the feedback path in addition to the actual observation vectors $\{\mathbf{y}_t^{(1)}, \dots, \mathbf{y}_t^{(R)}\}$. Incorporating the feedback, we define a new measurement vector

$$\boldsymbol{\eta}_t^{(r)} = \mathbf{B}_t^{(r)} \mathbf{y}_t^{(r)} + (\mathbf{I}_M - \mathbf{B}_t^{(r)}) \tilde{\mathbf{y}}_t^{(r)} \quad (18)$$

for the r th receiver, where $\mathbf{B}_t^{(r)}$ is an $M \times M$ diagonal matrix with the m th diagonal element $0 < \beta_t(m) < 1$, $m = 0, \dots, M - 1$, that determines the relative weight assigned to the respective sample of the current observation and the predicted observation vector at the t th observation. It is noted that a smaller $\beta_t(m)$ puts a lower emphasis on the current observation sample, which mitigates the effect of missing samples and strong additive noise. On the other hand, it results in a slower adaptation to any sudden changes in target trajectories [8]. Following the statistical model in (7), the weighted current observation vector can be modeled as

$$p(\mathbf{B}_t^{(r)} \mathbf{y}_t^{(r)} | \boldsymbol{\Phi}_t^{(r)}, \mathbf{B}_t^{(r)}, \boldsymbol{\theta}_{t,k}) \sim \mathcal{CN}(\mathbf{B}_t^{(r)} \boldsymbol{\Phi}_t^{(r)} \boldsymbol{\Psi}_t^{(r)} \mathbf{s}_t^{(r)}, \sigma_\epsilon^2 \mathbf{B}_t^{(r)} \mathbf{B}_t^{(r)H}). \quad (19)$$

Next, we investigate the statistical behavior of the predicted observation vector $\tilde{\mathbf{y}}_t^{(r)}$. As discussed earlier and since this paper attempts to evaluate and compare the performance bounds, we assume that the MTT filter also obtains an optimal unbiased solution. As such, the estimated target state vector can be represented as

$$\hat{\boldsymbol{\theta}}_{t,k} = \boldsymbol{\theta}_{t,k} + \boldsymbol{\vartheta}_{t,k}, \quad (20)$$

where $\boldsymbol{\vartheta}_{t,k}$ represents the estimation error obtained by exploiting the feedback structure. In this case, the samples of the predicted observation vector can be obtained through a known deterministic mapping, such that

$$\begin{aligned} \tilde{y}_t^{(r)}(m) &= \sum_{k=1}^K \psi(\hat{\boldsymbol{\theta}}_{t,k}, m) \\ &= \sum_{k=1}^K \psi(\boldsymbol{\theta}_{t,k} + \boldsymbol{\vartheta}_{t,k}, m), \end{aligned} \quad (21)$$

where $m = 0, \dots, M - 1$. It is noted that the statistical behavior of the predicted observation vector depends on the transformation of a Gaussian random variable in the parameter space to the measurement space, which is non-trivial to characterize [42]. Nonetheless, for a guaranteed convergence, the variance of the error in the estimated target state has to be upper-bounded by a small value. As such, we can

apply the first-order Taylor series approximation to obtain the following linearization of the predicted observation vector

$$\tilde{\mathbf{y}}_t^{(r)}(m) = \sum_{k=1}^K (\psi(\boldsymbol{\theta}_{t,k}, m) + \boldsymbol{\vartheta}_{t,k}^T \nabla \psi(\boldsymbol{\theta}_{t,k}, m)), \quad (22)$$

where $\nabla \psi(\boldsymbol{\theta}_{t,k}, m)$ is the gradient of the function calculated at $\boldsymbol{\theta}_{t,k}$. Following the sparse modeling in (3)–(7), we can model the predicted observation vector as

$$\tilde{\mathbf{y}}_t^{(r)} = \boldsymbol{\Psi}_t^{(r)} \mathbf{s}_t^{(r)} + \boldsymbol{\varsigma}_t^{(r)}, \quad (23)$$

where the m th sample of the error vector $\boldsymbol{\varsigma}_t^{(r)}$ is given by

$$\boldsymbol{\varsigma}_t^{(r)}(m) = \sum_{k=1}^K \boldsymbol{\vartheta}_{t,k}^T \nabla \psi(\boldsymbol{\theta}_{t,k}, m), \quad (24)$$

where $m = 0, \dots, M - 1$. The covariance matrix of the error vector $\boldsymbol{\varsigma}_t^{(r)}$ is obtained as $\mathbf{C}_{\boldsymbol{\varsigma}_t}^{(r)} \triangleq \mathbb{E}[\boldsymbol{\varsigma}_t^{(r)}(\boldsymbol{\varsigma}_t^{(r)})^H]$.

Having characterized the actual observation vectors $\mathbf{y}_t^{(r)}$ in (6) and the predicted observation vectors $\tilde{\mathbf{y}}_t^{(r)}$ in (23), and given the proposed relation in (18), we can express the conditional pdf of the effective measurement vectors $\boldsymbol{\eta}_t^{(r)}$ as

$$p(\boldsymbol{\eta}_t^{(r)} | \boldsymbol{\Phi}_t^{(r)}, \mathbf{B}_t^{(r)}, \boldsymbol{\theta}_{t,k}) \sim \mathcal{CN}(\tilde{\boldsymbol{\mu}}_t^{(r)}, \tilde{\mathbf{C}}_t^{(r)}), \quad (25)$$

where the mean vector is given by

$$\tilde{\boldsymbol{\mu}}_t^{(r)} = \mathbb{E}[\mathbf{B}_t^{(r)} \boldsymbol{\Phi}_t^{(r)} \boldsymbol{\Psi}_t^{(r)} \mathbf{s}_t^{(r)} + (\mathbf{I}_M - \mathbf{B}_t^{(r)}) \boldsymbol{\Psi}_t^{(r)} \mathbf{s}_t^{(r)}], \quad (26)$$

and the covariance matrix is obtained as

$$\tilde{\mathbf{C}}_t^{(r)} = \sigma_\epsilon^2 \mathbf{B}_t^{(r)} \mathbf{B}_t^{(r)H} + (\mathbf{I}_M - \mathbf{B}_t^{(r)}) \mathbf{C}_{\boldsymbol{\varsigma}_t}^{(r)} (\mathbf{I}_M - \mathbf{B}_t^{(r)})^H + 2\mathbf{B}_t^{(r)} \boldsymbol{\Sigma}_{\mathbf{y}, \tilde{\mathbf{y}}} (\mathbf{I}_M - \mathbf{B}_t^{(r)})^H, \quad (27)$$

where $\boldsymbol{\Sigma}_{\mathbf{y}, \tilde{\mathbf{y}}} \triangleq \mathbb{E}[\mathbf{y}_t^{(r)} \tilde{\mathbf{y}}_t^{(r)}]$ represents the cross-covariance matrix between the actual measurements and the predicted measurements. In the underlying problem, the additive error term introduced through the feedback, i.e., $\boldsymbol{\varsigma}_t^{(r)}$ defined in (23), is small compared to the additive noise term associated with the actual measurements, i.e., $\boldsymbol{\epsilon}_t^{(r)}$ defined in (6). Likewise, the cross-covariance term between the actual measurements and predicted measurements is also negligible owing to a small correlation coefficient between the two vectors, particularly in low SNR conditions and high percentage of missing samples. A numerical assessment of the correlation between the actual measurements and predicted measurements, for different SNR and varying ratios of missing samples, is presented later in Section V. Therefore, for the problem under consideration, the covariance matrix in (27) can be approximated as $\tilde{\mathbf{C}}_t^{(r)} \approx \sigma_\epsilon^2 \mathbf{B}_t^{(r)} (\mathbf{B}_t^{(r)})^H$.

Following (13), we can express the ij th block of the FIM obtained using the recursive feedback structure as

$$[\mathcal{I}(\boldsymbol{\theta}_t)]_{ij} = \sum_{r=1}^R 2 \operatorname{Re} \left[\frac{\partial \left(\tilde{\boldsymbol{\mu}}_t^{(r)} \right)^H}{\partial \boldsymbol{\theta}_{t,i}} \left(\tilde{\mathbf{C}}_t^{(r)} \right)^{-1} \frac{\partial \tilde{\boldsymbol{\mu}}_t^{(r)}}{\partial \boldsymbol{\theta}_{t,j}} \right], \quad (28)$$

and, following (17), the corresponding recursive FIM can be obtained as

$$[\mathcal{I}(\tilde{\boldsymbol{\theta}}_{t+1})]_{kk} = [\mathcal{I}(\boldsymbol{\theta}_{t+1})]_{kk} + \left[\mathbf{Q} + \mathbf{F}[\mathcal{I}(\tilde{\boldsymbol{\theta}}_t)]_{kk} \mathbf{F}^T \right]^{-1}. \quad (29)$$

The posterior bound on the variance of the target state estimates obtained using the feedback structure is given by the inverse of the corresponding block of the recursive FIM.

C. Discussion on convergence

The error in the estimated target state vector $\boldsymbol{\vartheta}_{t,k}$ causes two types of perturbations in the proposed recursive architecture: (a) When the magnitude of the error in the estimated target state vector $\boldsymbol{\vartheta}_{t,k}$ is smaller than the resolution of the dictionary matrix, the sparse representations of both the actual measurement and the predicted measurement share a common support. As such, this type of perturbation is corrected in the sparse reconstruction phase. Such a phenomenon is observed generally after the steady state is reached; (b) On the other hand, when the magnitude of the error in the estimated target state vector $\boldsymbol{\vartheta}_{t,k}$ is larger than the resolution of the dictionary matrix, the actual measurement vectors and the predicted measurement vectors constitute two multi-component sinusoids with different fundamental components. This results in a cardinality error. The MTT filter is capable of correcting for such cardinality errors and merging the multiple components as a single one, provided that the error ellipses of the target state estimates overlap with one another. For example, this process of cardinality management is described as ‘pruning’ in [43], where the Mahalanobis distance between a target state estimate and an error ellipse is used to merge/prune the estimates. As such, for guaranteed convergence, it is imperative that the magnitude of the error in target state estimates $\boldsymbol{\vartheta}_{t,k}$ is bounded within the error ellipse of the MTT filter.

D. Effect of relative weights

It can be inferred from (26) and (27) that the bounds on the instantaneous estimation error and the posterior error are functions of the relative weights. The preceding analysis can be used to determine an optimal value of the relative weights $0 < \beta_t(m) < 1$, $m = 0, \dots, M - 1$, for a given percentage of missing samples and a specified signal-to-noise ratio (SNR). This is elaborated further through numerical results in Section V.

For a case with no missing samples, i.e., when $\Phi_t^{(r)} = \mathbf{I}_M$, the mean vector is expressed as $\tilde{\boldsymbol{\mu}}_t^{(r)} = \mathbb{E}\{\Psi_t^{(r)} \mathbf{s}_t^{(r)}\}$, which is equal to the case with no missing samples and no feedback. In this case, the covariance matrix comprises smaller values, i.e., $\tilde{\mathbf{C}}_t^{(r)} \approx \sigma_\epsilon^2 \mathbf{B}_t^{(r)} (\mathbf{B}_t^{(r)})^H < \sigma_\epsilon^2 \mathbf{I}_M$, since $0 < \beta_t(m) < 1$, $m = 0, \dots, M-1$. Accordingly, by adopting the feedback structure, the bound on the variance of the target state estimates can actually be lowered compared to the case even without any missing samples. This is a remarkable improvement over the conventional sparsity-aware multi-sensor MTT algorithms.

In the following and as an application example, we consider the problem of tracking multiple ground moving targets in a passive multi-static radar (PMR) system exploiting Doppler-based observations. Simulation results are presented to validate the analysis in the preceding sections.

V. SIMULATION RESULTS

Consider the problem of tracking multiple ground moving targets in a PMR system exploiting Doppler-based observations as shown in Fig. 3. Such a PMR system typically comprises an illuminator of opportunity (e.g., Digital Audio Broadcast (DAB) and Digital Video Broadcast (DVB) stations, frequency modulation (FM) radio transmitter, and cellular mobile transmitter), a distributed network of Doppler sensors, and an information fusion center. Alternatively, a network comprising multiple spatially separated transmitters and a single Doppler sensor can be deployed. The former configuration with multiple sensors is more expensive; nonetheless, it is more flexible in configuring a favorable multi-static geometry by placing the sensors at appropriate positions around the available transmitter of opportunity [44].

In the simulations, we consider a PMR configuration as shown in Fig. 4, where a DAB broadcast station (Tx) is located at the origin of the coordinate system and transmits a cellular communication signal at a carrier frequency of 950 MHz, and 5 Doppler frequency measurement sensors (Rx) are distributed along a circle of radius 2.5 km from the transmitter. The region of interest is assumed to be a rectangular area bounded by $[-2500, 2500]^T$ m along both the x - and y -axes. The transmitter and the receivers are assumed stationary and their locations are assumed to be precisely known *a priori* at the fusion center.

Following the analysis in Section II, we consider $K = 2$ targets moving within the region of surveillance, which are initially located at $[-750, 0]^T$ m and $[750, 0]^T$ m and travel along linear trajectories with velocities $[30, 30]^T$ m/s and $[-30, 30]^T$ m/s, respectively, as shown in Fig. 4. The state vector of the k th target at the t th observation comprises its instantaneous position $\mathbf{p}_{t,k} \triangleq [p_{x,t,k}, p_{y,t,k}]^T$ and velocity $\mathbf{v}_k \triangleq [v_{x,k}, v_{y,k}]^T$ in the two-dimensional (2-D) Cartesian coordinate system, i.e., $\boldsymbol{\theta}_{t,k} = [\mathbf{p}_{t,k}^T, \mathbf{v}_k^T]^T$. The target dynamics are assumed to evolve according to a constant velocity linear Gaussian model described

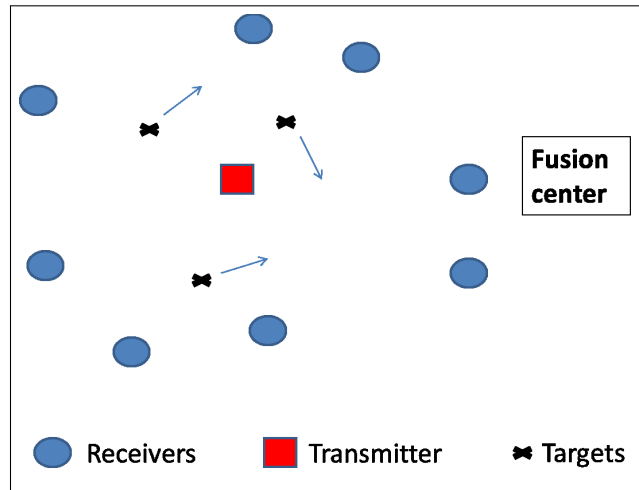


Fig. 3. Multi-static passive Doppler sensors network.

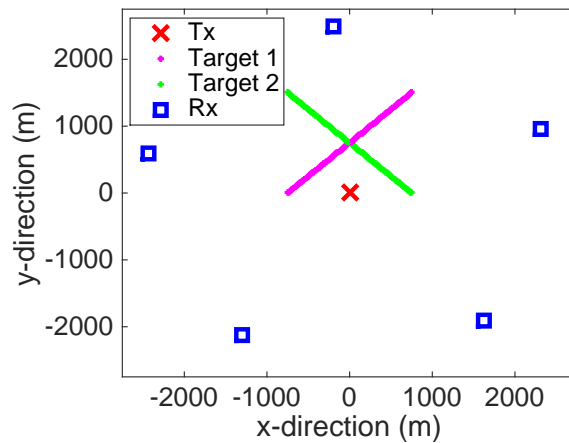


Fig. 4. True target trajectories and clutter.

in (1). As such, the state transition matrix \mathbf{F} is expressed as

$$\mathbf{F} = \begin{bmatrix} \mathbf{I}_2 & \Delta \mathbf{I}_2 \\ \mathbf{0}_2 & \mathbf{I}_2 \end{bmatrix}, \quad (30)$$

Δ is the sampling interval, and the covariance matrix of the process noise vector $\mathbf{w}_{t,k}$ can be expressed as [7]

$$\mathbf{Q} = \sigma_w^2 \begin{bmatrix} \frac{\Delta^4}{4} \mathbf{I}_2 & \frac{\Delta^3}{2} \mathbf{I}_2 \\ \frac{\Delta^3}{2} \mathbf{I}_2 & \Delta^2 \mathbf{I}_2 \end{bmatrix}. \quad (31)$$

The sensors report their respective observation vectors to the fusion center at an interval of $\Delta = 0.5$ sec. For each observation instant t , the observation vector comprises 512 samples corresponding to an

observation duration of 0.5 sec., and a sampling rate of $F_s = 1024$ Hz is considered to account for the maximum possible Doppler frequency measurement of $f_0 = 500$ Hz. As such, the m th sample of the signal received at the r th Doppler sensor is defined as a superposition of K complex exponentials corresponding to the radar returns from the detected targets during the t th interval, such that

$$\check{x}_t^{(r)}(m) = \sum_{k=1}^K s_{t,k}^{(r)} \exp(j2\pi f_{t,k}^{(r)} m), \quad (32)$$

where $s_{t,k}^{(r)}$ is the reflection coefficient corresponding to the k th target, $m = 0, \dots, M-1$ represent the discrete-time instants sampled at a rate of F_s over the t th interval, and $f_{t,k}^{(r)}$ is the bistatic Doppler frequency given by [45, 46]

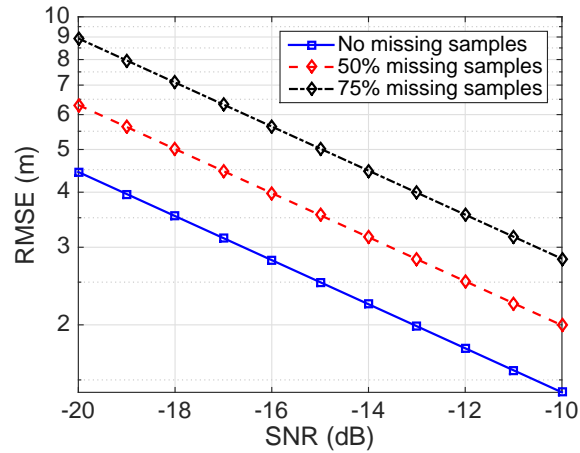
$$f_{t,k}^{(r)} = -\frac{\mathbf{v}_k^T}{\lambda} \left[\frac{\mathbf{p}_{t,k} - \mathbf{r}^{(r)}}{\|\mathbf{p}_{t,k} - \mathbf{r}^{(r)}\|_2} + \frac{\mathbf{p}_{t,k} - \mathbf{b}}{\|\mathbf{p}_{t,k} - \mathbf{b}\|_2} \right], \quad (33)$$

where \mathbf{b} and $\mathbf{r}^{(r)}$ are the vectors representing the 2-D locations of the transmitter and the r th sensor, respectively.

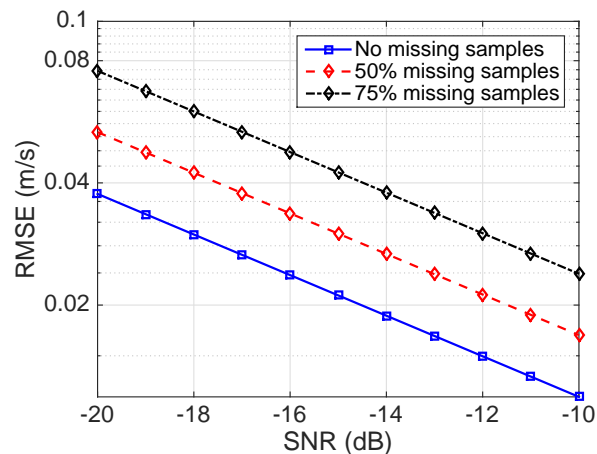
In this example, the target state space can be represented as an N -dimensional sparse vector $\mathbf{s}_t^{(r)}$, where each element in $\mathbf{s}_t^{(r)}$ is uniquely associated with a discrete point in the position-velocity space. Following the sparse signal reconstruction model in (3), the sparse decomposition of $\check{\mathbf{x}}_t^{(r)}$ can be expressed as $\check{\mathbf{x}}_t^{(r)} = \mathbf{\Psi}_t^{(r)} \mathbf{s}_t^{(r)}$, where the basis or the dictionary matrix $\mathbf{\Psi}_t^{(r)}$ is defined in the discrete position-velocity space.

The lower bound on the root-mean-square error (RMSE) on the instantaneous estimation of target position and velocity, assuming different proportion of missing samples, is compared in Fig. 5. As discussed in Section III, the bounds on the RMSE of the position and velocity estimates increase by a factor of $\sqrt{M/(M-L)}$, i.e., approximately 1.41 for 50% missing samples and 2.00 for 75% missing samples.

The posterior bound is compared in Fig. 6 for three different proportions of missing samples while the input SNR is maintained at -15 dB. The effect of strong additive Gaussian noise and high proportion of missing samples is relatively lower in the steady-state posterior bound compared to the bound on the instantaneous state estimation. For example, as shown in Fig. 6, the posterior bound on the standard deviation of position estimate at -15 dB and 50% missing samples is approximately equal to 1 m, which is a significant reduction from 3.4 m before tracking. This is the motivation behind the recursive learning architecture presented in [8]. It is noted that the tracking performance also depends on the variance of the process noise variance, which is set to be $\sigma_w^2 = 1$ in this simulation example. Next, we present the posterior bound on the RMSE of the estimated target states at the k th observation by evaluating the



(a)

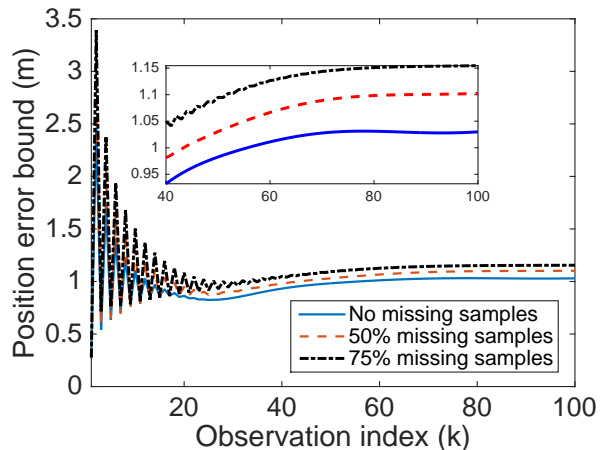


(b)

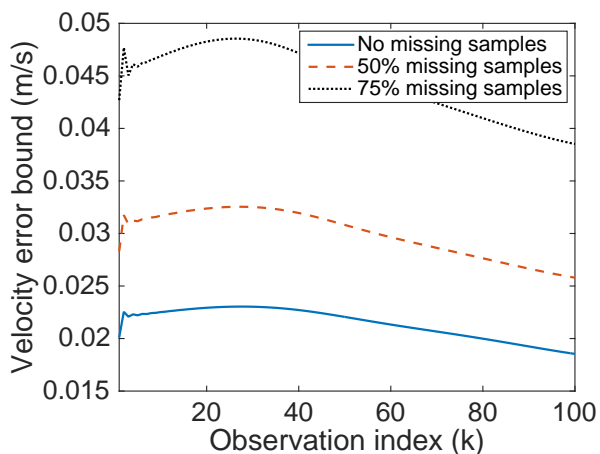
Fig. 5. Error bounds on the estimates of (a) position; and (b) velocity.

inverse of the posterior FIM derived in (29). It is noted that the analysis in (27) requires a negligible correlation between the actual measurements and the predicted measurements used for recursion. This is verified through a numerical example in Fig. 7. For all values of the SNR and the ratio of missing samples considered, the resulting correlation coefficient is very low. It is interesting to note that the correlation coefficient is lower in the more challenging scenarios where the input SNR is low or the ratio of the missing samples is high.

The lower bound on the RMSE of the instantaneous estimation of target position and velocity achieved using the feedback structure is compared in Fig. 8 against the conventional method, assuming 50% missing samples. As analytically evaluated in Section V and by exploiting the feedback structure, we lower the



(a)



(b)

Fig. 6. Posterior error bounds on the estimates of (a) position; and (b) velocity.

bound on the variance of the instantaneous target state estimates. In fact, by properly choosing the value of $\mathbf{B}_t^{(r)}$, a bound smaller than the case with no missing samples can be achieved. In this simulation example, we use $\mathbf{B}_t^{(r)} = 0.75\mathbf{I}_M$.

Next, we compare the posterior bound on the RMSE of the estimated target states at the k th observation achieved, respectively, by exploiting the conventional approach and the recursive feedback method. The posterior bound is compared in Fig. 9 for 50% missing samples and an input SNR of -15 dB. It is noted that the tracking performance is significantly improved by exploiting the feedback structure both in terms of the rate of convergence and the accuracy at the steady state.

For a given percentage of missing samples and SNR, the emphasis on feedback structure determines

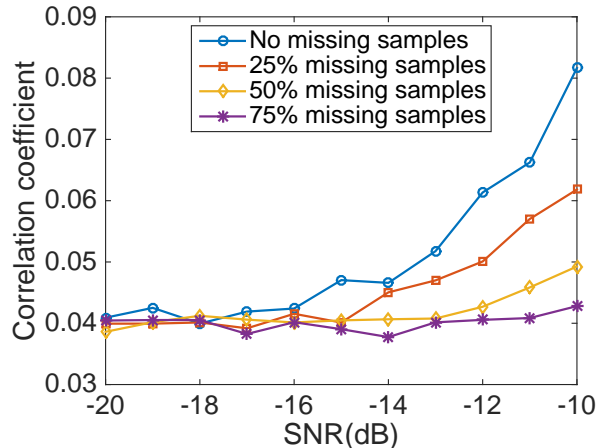


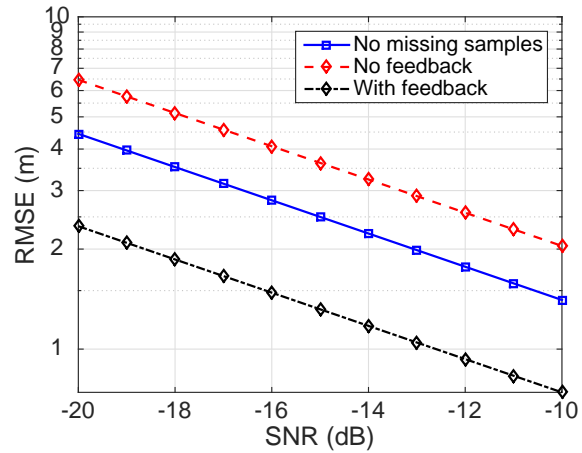
Fig. 7. Correlation between actual measurements and predicted measurements.

the performance improvement that can be achieved through recursive learning. The effect of varying the relative weight for different proportions of missing samples is shown in Fig. 10. It is evident that the estimation error increases when a lower weight is placed on the predicted observation vector. This effect becomes more prominent as the percentage of missing samples is increased.

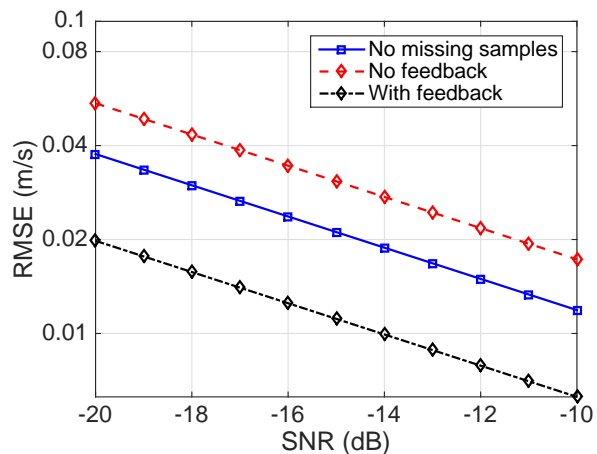
Next, we compare the posterior error bound on the RMSE of the estimated target states at the k th observation for different values of relative weights, while the percentage of missing samples is maintained at 50% and an input SNR of -15 dB is considered in all three cases. As illustrated in Fig. 11, the lower the relative weight on the predicted observation vector is, the larger the posterior error bound gets, and it also takes a longer time to reach for the steady state. However, it is important to note, particularly for highly maneuvering targets, that a higher relative weight on the predicted observation vector delays the adaptation to any changes in the target trajectory.

VI. CONCLUSIONS

In this paper, we have analytically derived and compared the Cramer-Rao type performance bounds for two algorithmic structures for sparsity-aware multi-sensor MTT. First, we analytically evaluated the performance degradation of the conventional two-step sequential architecture that cascades the group sparse reconstruction algorithm and the MTT algorithm in a situation where the observation suffers from a high proportion of missing samples. Next, we derived the performance bounds for a recently developed technique for sparsity-aware multi-sensor MTT which deploys a recursive feedback mechanism such that the group sparse reconstruction algorithm also benefits from the *a priori* knowledge about the target



(a)



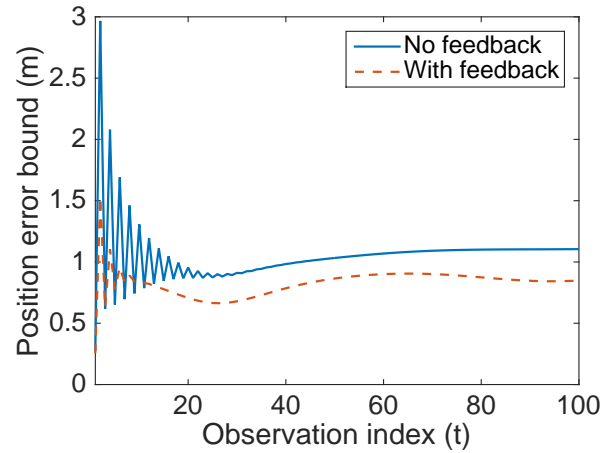
(b)

Fig. 8. Error bounds on the estimates of (a) position; and (b) velocity.

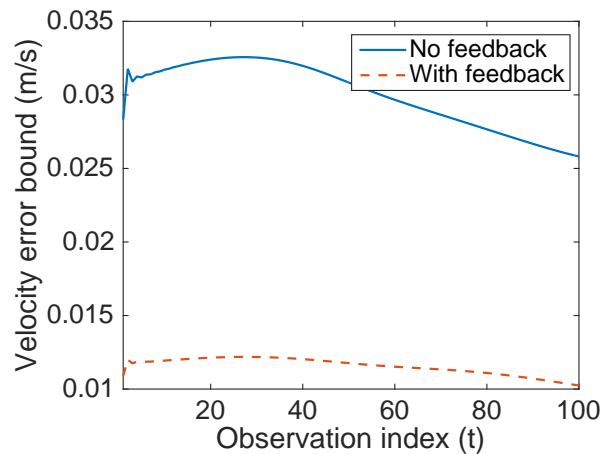
dynamics. Through an application example in the context of multisensor MTT in PMR systems, we have shown that the recursive learning structure outperforms the conventional approach, when the measurement vectors are corrupted by a high percentage of missing samples and strong additive noise.

REFERENCES

- [1] S. Subedi, Y. D. Zhang, M. G. Amin, and B. Himed, "Cramer-Rao type bounds for sparsity-aware multi-target tracking in multi-static passive radar," in *Proc. IEEE Radar Conf.*, Philadelphia, PA, May 2016.
- [2] N. Vaswani, "Kalman filtered compressed sensing," in *Proc. IEEE ICIP*, San Diego, CA, Oct. 2008, pp. 893–896.
- [3] D. Angelosante, J. A. Bazerque, and G. B. Giannakis, "Online adaptive estimation of sparse signals: where RLS meets the ℓ_1 -Norm," *IEEE Trans. Signal Process.*, vol. 58, no. 7, pp. 3436–3447, July 2010.



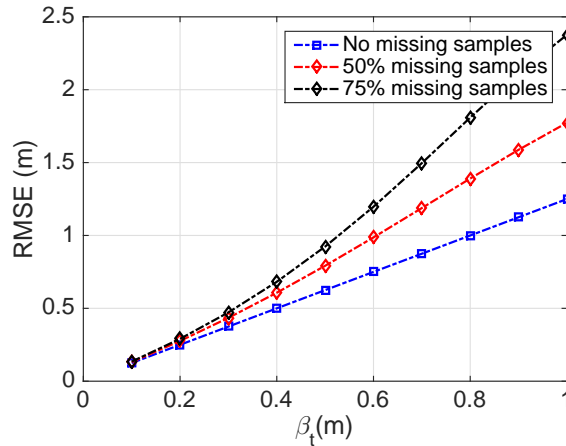
(a)



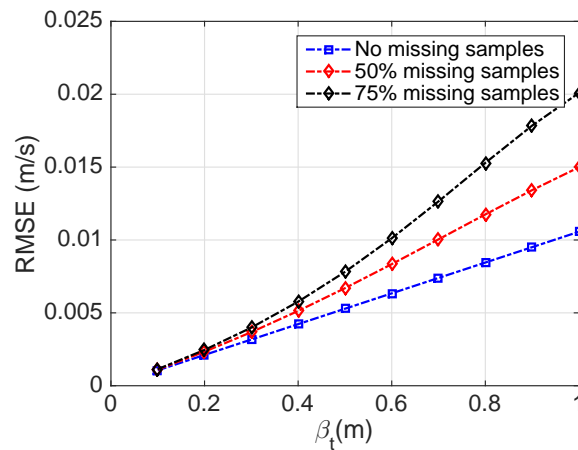
(b)

Fig. 9. Posterior error bounds on the estimates of (a) position; and (b) velocity.

- [4] E. Masazade, M. Fardad, and P. K. Varshney, "Sparsity-promoting extended Kalman filtering for target tracking in wireless sensor networks," *IEEE Signal Process. Lett.*, vol. 19, no. 12, pp. 845–848, Dec. 2012.
- [5] S. Farahmand, G. B. Giannakis, G. Leus, and Z. Tian, "Sparsity-aware Kalman tracking of target signal strengths on a grid," in *Proc. FUSION*, Chicago, IL, July 2011, pp. 1–6.
- [6] E. Karseras, K. Leung, and W. Dai, "Tracking dynamic sparse signals using hierarchical Bayesian Kalman filters," in *Proc. IEEE ICASSP*, Vancouver, Canada, May 2013, pp. 6546–6550.
- [7] S. Subedi, Y. D. Zhang, M. G. Amin, and B. Himed, "Group sparsity based multi-target tracking in passive multi-static radar systems using Doppler-only measurements," *IEEE Trans. Signal Process.*, vol. 64, no. 14, pp. 3619–3634, July 2016.
- [8] S. Subedi, Y. D. Zhang, and M. G. Amin, "Sparse reconstruction of multi-component Doppler signature exploiting target dynamics," in *Proc. IEEE CAMSAP Workshop*, Cancun, Mexico, Dec. 2015, pp. 73–76.



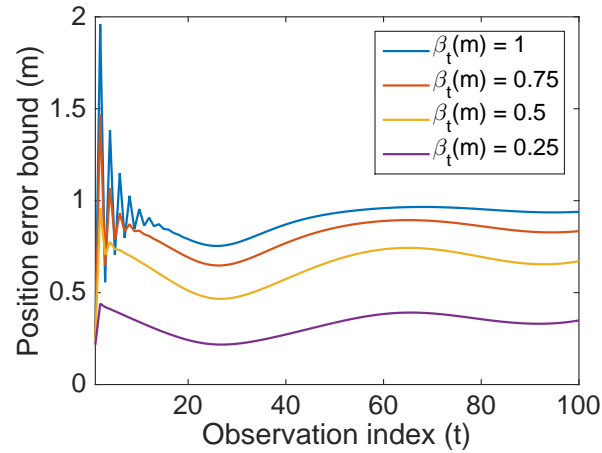
(a)



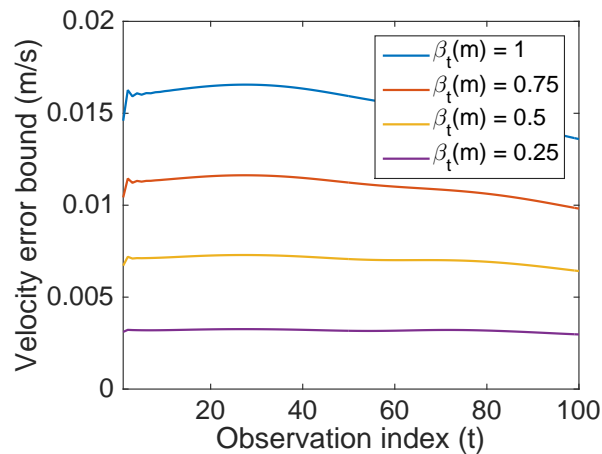
(b)

Fig. 10. Effect of relative weights on the error bounds on the instantaneous estimates of (a) position; and (b) velocity.

- [9] D. Schuhmacher, B. T. Ho, and B. N. Ho, "A consistent metric for performance evaluation of multi-object filters," *IEEE Trans. Signal Process.*, vol. 56, no. 8, pp. 3447–3457, Aug. 2008.
- [10] H. Van Trees and K. Bell, *Bayesian Bounds for Parameter Estimation and Nonlinear Filtering/Tracking*, Wiley-IEEE Press, 2007.
- [11] P. Tichavsky, C. H. Muravchik, and A. Nehorai, "Posterior Cramer-Rao bounds for discrete-time nonlinear filtering," *IEEE Trans. Signal Process.*, vol. 46, no. 5, pp. 1386–1396, May 1998.
- [12] K. Punithakumar, T. Kirubarajan, and M. L. Hernandez, "Multisensor deployment using PCRLBS, incorporating sensor deployment and motion uncertainties," *IEEE Trans. Aerosp. Electron. Syst.*, vol. 42, no. 4, pp. 1474-1485, Oct. 2006.
- [13] R. Tharmarasa, T. Kirubarajan, and M. L. Hernandez, "Large-scale optimal sensor array management for multitarget tracking," *IEEE Trans. Syst., Man, Cybern. C, Appl. Rev.*, vol. 37, no. 5, pp. 803-814, Sep. 2007.



(a)



(b)

Fig. 11. Effect of relative weights on the posterior error bounds on the estimates of (a) position; and (b) velocity.

- [14] R. Tharmarasa, T. Kirubarajan, M. L. Hernandez, and A. Sinha, "PCRLB-based multisensor array management for multi-target tracking," *IEEE Trans. Aerosp. Electron. Syst.*, vol. 43, no. 2, pp. 539-555, Apr. 2007.
- [15] L. Zuo, R. Niu and P. K. Varshney, "Conditional posterior Cramer-Rao lower bounds for nonlinear sequential Bayesian estimation," *IEEE Trans. Signal Process.*, vol. 59, no. 1, pp. 1-14, Jan. 2011.
- [16] Y. Zheng, O. Ozdemir, R. Niu and P. K. Varshney, "New conditional posterior Cramer-Rao lower bounds for nonlinear sequential Bayesian estimation," *IEEE Trans. Signal Process.*, vol. 60, no. 10, pp. 5549-5556, Oct. 2012.
- [17] J. K. Nielsen, M. G. Christensen, and S. H. Jensen, "On compressed sensing and the estimation of continuous parameters from noisy observations," in *Proc. IEEE ICASSP*, Kyoto, Japan, Mar. 2012, pp. 3609-3612.
- [18] Y. Bar-Shalom and X. Li, *Multitarget-Multisensor Tracking: Principles and Techniques*, New York, NY: YBS, 1995.

- [19] E. Mazor, A. Averbuch, Y. Bar-Shalom, and J. Dayan, "Interacting multiple model methods in target tracking: a survey," *IEEE Trans. Aerosp. Electron. Syst.*, vol. 34, no. 1, pp. 103–123, Jan. 1998.
- [20] R. P. S. Mahler, "'Statistics 101' for multisensor, multitarget data fusion," *IEEE Aerosp. Electron. Syst. Mag.*, vol. 19, no. 1, pp. 53–64, Jan. 2004.
- [21] R. Mahler, "'Statistics 102' for multisource-multitarget detection and tracking," *IEEE J. Sel. Topics Signal Process.*, vol. 7, no. 3, pp. 376–389, Jun. 2013.
- [22] T. E. Fortmann, Y. Bar-Shalom, and M. Scheffe, "Sonar tracking of multiple targets using joint probabilistic data association," *IEEE J. Ocean. Eng.*, vol. 8, no. 3, pp. 173–184, July 1983.
- [23] R. Mahler, "PHD filters of higher order in target number," *IEEE Trans. Aerosp. Electron. Syst.*, vol. 43, no. 4, pp. 1523–1543, Oct. 2007.
- [24] B. Ristic and A. Farina, "Recursive Bayesian state estimation from Doppler-shift measurements," in *Proc. IEEE Int. Conf. Intell. Sensors, Sensor Networks and Info. Process.*, Adelaide, Australia, Dec. 2011.
- [25] D. L. Donoho, "Compressed sensing," *IEEE Trans. Inf. Theory*, vol. 52, no. 4, pp. 1289–1306, Apr. 2006.
- [26] C. Rich, "Multitask learning," *Machine Learning*, vol. 28, no. 1, pp. 41–75, Sept. 1997.
- [27] Y. C. Eldar, P. Kuppinger, and H. Bolcskei, "Block-sparse signals: uncertainty relations and efficient recovery," *IEEE Trans. Signal Process.*, vol. 58, no. 6, pp. 3042–3054, June 2010.
- [28] M. Carlin, P. Rocca, G. Oliveri, F. Viani, and A. Massa, "Directions-of-arrival estimation through Bayesian compressive sensing strategies," *IEEE Trans. Antennas Propagat.*, vol. 61, no. 7, pp. 3828–3838, 2013.
- [29] Q. Shen, W. Liu, W. Cui, S. Wu, Y. D. Zhang, and M. G. Amin, "Low-complexity wideband direction-of-arrival estimation based on co-prime arrays," *IEEE/ACM Trans. Audio, Speech and Language Process.*, vol. 23, no. 9, pp. 1445–1456, Sept. 2015.
- [30] S. Liu, S. Kar, M. Fardad, and P. K. Varshney, "Sparsity-aware sensor collaboration for linear coherent estimation," *IEEE Trans. Signal Process.*, vol. 63, no. 10, pp. 2582–2596, May 2015.
- [31] E. V. D. Berg and M. Friedlander, "Probing the Pareto frontier for basis pursuit solutions," *SIAM J. Sci. Computing*, vol. 31, no. 2, pp. 890–912, 2008.
- [32] M. Yuan and Y. Lin, "Model selection and estimation in regression with grouped variables," *J. Royal Statist. Soc. Series B*, vol. 68, no. 1, pp. 49–67, 2006.
- [33] L. Zelnik-Manor, K. Rosenblum, and Y. C. Eldar, "Sensing matrix optimization for block-sparse decoding," *IEEE Trans. Signal Process.*, vol. 59, no. 9, pp. 4300–4312, Sept. 2011.
- [34] S. Ji, D. Dunson, and L. Carin, "Multitask compressive sensing," *IEEE Trans. Signal Process.*, vol. 57, no. 1, pp. 92–106, Jan. 2009.
- [35] Q. Wu, Y. D. Zhang, M. G. Amin, and B. Himed, "Complex multitask Bayesian compressive sensing," in *Proc. IEEE ICASSP*, Florence, Italy, May 2014.
- [36] R. Mahler, "The multisensor PHD filter: I. General solution via multitarget calculus," in *Proc. SPIE*, vol. 7336, Orlando, FL, Apr. 2009.
- [37] S. M. Kay, *Fundamentals of Statistical Signal Processing: Estimation Theory*, Upper Saddle River, NJ: Prentice Hall PTR, 1993.

- [38] D. S. Pham and A. M. Zoubir, "Analysis of multicomponent polynomial phase signals," *IEEE Trans. Signal Process.*, vol. 55, no. 1, pp. 56–65, Jan. 2007.
- [39] C. Wei, Q. He, and R. S. Blum, "Cramer-Rao bound for joint location and velocity estimation in multi-target non-coherent MIMO radars," in *Proc. IEEE CISS*, Princeton, NJ, Mar. 2010, pp. 1–6.
- [40] H. Tong, H. Zhang, H. Meng, and X. Wang, "The recursive form of error bounds for RFS state and observation With $P_d < 1$," *IEEE Trans. Signal Process.*, vol. 61, no. 10, pp. 2632–2646, May 2013.
- [41] C. Hue, J. -P. C. Le, and P. Perez, "Posterior Cramer-Rao bounds for multi-target tracking," *IEEE Trans. Aerosp. Electron. Syst.*, vol. 42, no. 1, pp. 37–49, Jan. 2006.
- [42] S. Kumar, V. K. Goyal, and S. E. Sarma, "Efficient parametric signal estimation from samples with location errors," *IEEE Trans. Signal Process.*, vol. 61, no. 21, pp. 5285–5297, Nov. 2013.
- [43] B. Vo and W. K. Ma, "The Gaussian mixture probability hypothesis density filter," *IEEE Trans. Signal Process.*, vol. 54, no. 11, pp. 4091–4104, Nov. 2006.
- [44] G. Battistelli, L. Chisci, S. Morrocchi, F. Papi, A. Farina, and A. Graziano, "Robust multi-sensor multi-target tracker with application to passive multistatic radar tracking," *IEEE Trans. Aerosp. and Electron. Syst.*, vol. 48, no. 4, pp. 3450–3472, Oct. 2012.
- [45] Y. D. Zhang and B. Himed, "Moving target parameter estimation and SFN ghost rejection in multi-static passive radar," in *Proc. IEEE Radar Conf.*, Ottawa, Canada, Apr. 2013, pp. 1–5.
- [46] S. Subedi, Y. D. Zhang, M. G. Amin, and B. Himed, "Motion parameter estimation of multiple ground moving targets in multi-static passive radar systems," *EURASIP J. Adv. Signal Process.*, vol. 2014, no. 157, pp. 1–14, Oct. 2014.